

# Apparent anomalous diffusion and non-Gaussian distributions in a simple mobile–immobile transport model with Poissonian switching

Timo J. Doerries<sup>†</sup>, Aleksei V. Chechkin<sup>†,‡,§</sup> and Ralf Metzler<sup>†</sup>

<sup>†</sup>Institute of Physics & Astronomy, University of Potsdam, 14476 Potsdam, Germany

<sup>‡</sup>Faculty of Pure and Applied Mathematics, Hugo Steinhaus Center, Wrocław University of Science and Technology, Wyspińskiego 27, 50-370 Wrocław, Poland

<sup>§</sup>Akhiezer Institute for Theoretical Physics, 61108 Kharkov, Ukraine

**Abstract.** We analyse mobile-immobile transport of particles that switch between the mobile and immobile phases with finite rates. Despite this seemingly simple assumption of Poissonian switching we unveil a rich transport dynamics including significant transient anomalous diffusion and non-Gaussian displacement distributions. Our discussion is based on experimental parameters for tau proteins in neuronal cells, but the results obtained here are expected to be of relevance for a broad class of processes in complex systems. Concretely, we obtain that when the mean binding time is significantly longer than the mean mobile time, transient anomalous diffusion is observed at short and intermediate time scales, with a strong dependence on the fraction of initially mobile and immobile particles. We unveil a Laplace distribution of particle displacements at relevant intermediate time scales. For any initial fraction of mobile particles, the respective mean squared displacement displays a plateau. Moreover, we demonstrate a short-time cubic time dependence of the mean squared displacement for immobile tracers when initially all particles are immobile.

## 1. Introduction

Already in the 1960ies there was considerable interest in the transport of chemical tracers, especially pesticides, nitrates, or heavy metals through water-carrying layers of the soil [1]. A typical description for such contaminant transport was the diffusion-advection equation (sometimes called convective-dispersive equation) [2]

$$\frac{\partial}{\partial t}C(x, t) = D\frac{\partial^2}{\partial x^2}C(x, t) - v\frac{\partial}{\partial x}C(x, t), \quad (1)$$

where  $C(x, t)$  is the contaminant concentration at distance  $x$  after time  $t$ ,  $v$  is an advection velocity chosen as zero in the following, and  $D$  the diffusion constant (dispersion coefficient typically measured in units of  $\text{cm}^2/\text{day}$ ). Measurements revealed, however, that not all of the contaminant concentration was mobile at any given time, but that a fraction could be (transiently) trapped in stagnant volumes. Building on earlier models by Deans [3] and Coats and Smith [4], van Genuchten and Wierenga analyse the

exchange between a mobile ( $C_m(x, t)$ ) and immobile ( $C_{im}(x, t)$ ) fraction [5]. In many geophysical systems equations of the type (1) are modified to account for anomalous transport, in which molecular transport no longer follows the linear time dependence  $\langle \Delta x^2(t) \rangle = \langle x^2(t) \rangle - \langle x(t) \rangle^2 = 2Dt$  of Brownian motion, but follows laws of the type  $\langle \Delta x^2(t) \rangle = 2D_\alpha t^\alpha$ , for which  $\alpha \neq 1$  [6]. Indeed such transport anomalies were found on large field experiments, up to kilometre scales [7, 8]. In such systems the mobile-immobile transport model is replaced by models in which generalised transport terms are incorporated [9, 10]. This type of models, in contrast to equation (1), is characterised by non-Gaussian distributions [6].

Motivated by concrete biological examples we here study a seemingly simple version of the mobile-immobile transport model, in which particles switch between a freely diffusive phase and an immobile, stagnant phase. Even for the Poissonian switching dynamics considered here between the mobile and immobile phases and for biologically relevant parameters, we demonstrate the existence of a significant, transient anomalous-diffusive regime with distinct non-Gaussian displacement distribution.

In fact, various components of biological cells, including tau proteins, synaptic vesicles in hippocampal neurons, glucocorticoid receptors, calcium sensing proteins and transcription factors at the junction of the endoplasmic reticulum and the plasma membrane undergo diffusion with intermittent immobilisation [11–18]. We here focus on tau proteins, that intermittently bind to microtubules in axons of neuronal cells and are then immobilised, as schematically depicted in figure 1. Tau proteins stabilise microtubules that give structure to cells [19]. Alzheimer’s disease is associated with tau proteins losing the ability to bind to microtubules [19, 20]. This effectively destabilises the microtubules and leads to neurodegeneration [19, 20]. Due to the extremely elongated shape of the axon the motion of tau proteins can be effectively described in one dimension [11]. If the immobilisation time follows an exponential distribution with mean  $\tau_{im}$  and tracers immobilise with rate  $\tau_m^{-1}$ , i.e., a Poissonian dynamics, as assumed in [11], the motion can be described by the mobile-immobile model

$$\begin{aligned} \frac{\partial}{\partial t} n_m(x, t) &= -\frac{1}{\tau_m} n_m(x, t) + \frac{1}{\tau_{im}} n_{im}(x, t) + D \frac{\partial^2}{\partial x^2} n_m(x, t) \\ \frac{\partial}{\partial t} n_{im}(x, t) &= -\frac{1}{\tau_{im}} n_{im}(x, t) + \frac{1}{\tau_m} n_m(x, t). \end{aligned} \quad (2)$$

Here  $n_m(x, t)$  and  $n_{im}(x, t)$  denote the line densities of mobile and bound tau proteins, respectively, with physical dimension [1/length]. The diffusion coefficient of the mobile tracers is  $D$ . Since we are dealing with a system of non-interacting particles, we use a probabilistic formulation according to which the total concentration  $n_{tot}(x, t) = n_m(x, t) + n_{im}(x, t)$  is normalised to unity,  $\int_{-\infty}^{\infty} n_{tot}(x, t) dx = 1$ . The line densities  $n_m(x, t)$  and  $n_{im}(x, t)$  are then the respective fractions. Equations (2) were analysed in three dimensions for an equilibrium fraction of initially mobile tracers, finding Fickian yet non-Gaussian diffusion [21]. Accordingly, the mean squared displacement (MSD) of the total concentration  $n_{tot}$  grows linearly at all times, and under certain conditions a non-Gaussian distribution emerges [21].

Such Fickian yet non-Gaussian diffusion has been shown to occur for the motion of colloidal beads on phospholipid bilayer tubes, molecules at surfaces, and colloids in a dense matrix of micropillars, where the colloids can get trapped in pockets [22–24]. Fickian-yet non-Gaussian diffusion with a finite correlation time beyond which the displacement probability density function (PDF) crosses over to a Gaussian with an effective diffusivity, arises in diffusing-diffusivity models, in which the diffusivity of individual tracers varies stochastically over time [25–30]. Direct examples for such randomly evolving diffusion coefficients (mobilities) are indeed known from lipids in protein-crowded bilayer membranes [31], shape-shifting protein molecules [32], or (de)polymerising oligomer chains [33, 34]. In other systems an intermittent plateau emerges in the MSD, for instance, for two-dimensional fluids confined in a random matrix of obstacles or a porous cavity, in which trapping in finite pockets plays a key role [35–37]. We also mention plateaus in the MSD of both two- and three-dimensional isotropic Lennard-Jones binary liquids [38]. In most of the systems mentioned here the PDF crosses over from an exponential (Laplace) PDF to a Gaussian. In the following we explicitly show how a Laplace distribution with fixed scale parameters arises at intermediate time scales in our mobile-immobile model, paired with transient anomalous diffusion.

In what follows we consider three initial conditions, an equilibrium fraction of mobile tracers and a scenario in which initially all tracers are mobile or immobile. These experimentally feasible situations significantly change the diffusion at short and intermediate time scales, at which apparent anomalous diffusion arises with slow-down and plateau-like behaviour, or ballistic diffusion, respectively. Together with the transient non-Gaussian displacement PDF this behaviour is remarkably rich, given the simplicity of the governing equation (2). We individually analyse the motion of the mobile and immobile population of tracers, made possible by the formulation of separate densities for mobile and immobile particles in this modelling approach. One physical incentive to do so is that the function of the tau proteins depends on their binding state [19]. Only bound tau proteins stabilise microtubules, or transcription factors modulate gene expression when bound to the DNA [15, 19]. In some situations only the mobile or immobile tracers can be measured. An example is given by combining total internal reflection fluorescence microscopy with fluorescently labelled single stranded DNA, that binds to the microscope cover slip [39].

We present general results for the mobile and immobile concentrations and the MSD for arbitrary fractions of initially mobile tracers in section 2. Sections 3, 4, and 5 present concrete results and detailed discussions for different fractions of initial mobile particle concentrations; respectively, we start with the cases when all tracers are initially mobile and immobile and commence with an equilibrium fraction of mobile tracers. We conclude in section 6.

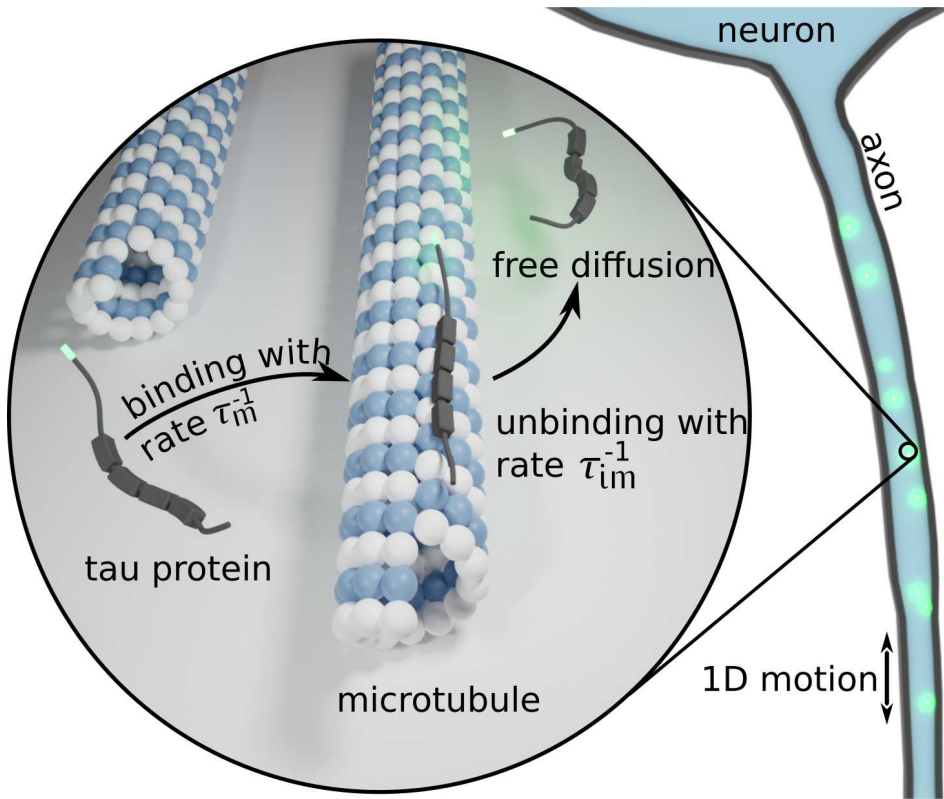


**Figure 1.** Schematic of tau protein dynamics in axons of neuronal cells. Diffusing tau proteins bind to longitudinally aligned microtubules inside the axon with the rate  $\tau_m^{-1}$ . Upon binding they remain immobile for the average duration  $\tau_{im}$  and unbind with the rate  $\tau_{im}^{-1}$ . The green markers represent fluorescent proteins attached to the tau proteins. Due to the elongated shape of the axons the tau protein dynamic can effectively be described in one dimension. In our model we assume a homogeneous binding site density.

## 2. Model and general solutions

We consider the mobile-immobile model equations (2) for the initial conditions  $n_m(x, 0) = f_m \delta(x)$  and  $n_{im}(x, 0) = f_{im} \delta(x)$ , where  $f_m$  and  $f_{im}$  denote the fractions of initially mobile and immobile tracers, respectively, with the normalisation  $f_m + f_{im} = 1$ . This formulation is suitable for typical single-particle tracking experiments used in biological and soft matter systems. They are also relevant for geophysical experiments, in which point-like injection of tracers are used. In this section we keep the fractions  $f_m$  and  $f_{im}$  arbitrary and choose specific values in the following three sections.

In what follows, we use the concrete parameters  $D = 13.9 (\mu\text{m})^2/\text{sec}$ ,  $\tau_m = 0.16 \text{ sec}$ , and  $\tau_{im} = 7.7 \text{ sec}$  from [11] in all figures and neglect the vanishingly small advection velocity  $v = 0.002 \mu\text{m}/\text{sec}$ .<sup>‡</sup> Let us briefly address the experimental origin of the time scale separation between  $\tau_m$  and  $\tau_{im}$ . From single particle tracking experiments of single-stranded DNA or tau proteins, immobilisation times during the particle motion can be

<sup>‡</sup> The slow directed motion only plays a role when very long times are considered [11, 40, 41].

extracted [12, 39]. The experiments for the tau proteins in [12] provide two-dimensional information and revealed relatively short residence times of the tau proteins on the microtubules, as compared to mobile times [12]. In contrast, the fluorescence decay after photoactivation (FDAP) experiment in one dimension along the axon direction, here denoted as the  $x$  variable, reveal long residence times and short mobile periods:  $\tau_{\text{im}} \approx 48\tau_{\text{m}}$  [11]. This seeming contradiction can be resolved when examining more closely the two-dimensional trajectories in the supplementary material of [12]. Namely, the microtubules inside the axon are aligned in parallel to the axon axis, as also shown in our schematic 1. While a single binding event is short, an unbound particle quickly rebinds to a parallel, close-by microtubule after a short distance covered by diffusion perpendicular to the axon axis. This perpendicular motion does not contribute to the one-dimensional motion in  $x$  direction and thus, while individual binding times are relatively short, *effective* binding times appear much longer in the projection to one dimension. Since we are only interested in the one-dimensional motion we use the parameters of [11] and hence long immobilisation times.

### 2.1. Mobile and immobile concentration profiles

We consider the Fourier-Laplace transform of the concentrations and solve for  $n_{\text{m}}(k, s)$ ,  $n_{\text{im}}(k, s)$  and  $n_{\text{tot}}(k, s)$  in expressions (A.1) and (A.2), in which the Fourier wave number  $k$  corresponds to the distance  $x$  in real space, and the Laplace variable  $s$  is conjugated to time  $t$ , see Appendix A for details. We denote functions in Fourier or Laplace space solely by replacing the explicit dependencies on the respective arguments. The relations in Fourier-Laplace domain can be Fourier-inverted, and we obtain the expressions

$$n_{\text{m}}(x, s) = \left( f_{\text{m}} + f_{\text{im}} \frac{1}{1 + s\tau_{\text{im}}} \right) \frac{1}{\sqrt{4\phi(s)D}} e^{-\sqrt{\phi(s)/D}|x|} \quad (3)$$

$$n_{\text{im}}(x, s) = \left( f_{\text{m}} + f_{\text{im}} \frac{1}{1 + s\tau_{\text{im}}} \right) \frac{\tau_{\text{im}}/\tau_{\text{m}}}{1 + s\tau_{\text{im}}} \frac{1}{\sqrt{4\phi(s)D}} e^{-\sqrt{\phi(s)/D}|x|} + f_{\text{im}} \frac{\tau_{\text{im}}}{1 + s\tau_{\text{im}}} \delta(x) \quad (4)$$

$$n_{\text{tot}}(x, s) = \frac{f_{\text{m}} + f_{\text{im}} \frac{1}{1 + s\tau_{\text{im}}}}{s} \phi(s) \frac{1}{\sqrt{4\phi(s)D}} e^{-\sqrt{4\phi(s)/D}|x|} + f_{\text{im}} \frac{\tau_{\text{im}}}{1 + s\tau_{\text{im}}} \delta(x) \quad (5)$$

as functions of  $x$  and  $s$  with  $\phi(s) = s[1 + \tau_{\text{im}}\tau_{\text{m}}^{-1}/(1 + s\tau_{\text{im}})]$ . These expressions are valid for all  $s$  and hence for all times  $t$ . A numerical Laplace inversion then provides the densities for any specified time. Remarkably, it turns out that the density of mobile tracers, that were initially immobile, is proportional to the density of immobile tracers, that were initially mobile. This can be seen by setting  $f_{\text{m}} = 0$  or  $f_{\text{im}} = 0$  in (3) and (4), respectively. This proportionality holds for all  $s$  and hence at all times. We obtain the long-time Gaussian limit of the full concentration in Appendix B.3,

$$n_{\text{tot}}(x, t) \sim \frac{1}{\sqrt{4\pi D_{\text{eff}}t}} \exp\left(-\frac{x^2}{4D_{\text{eff}}t}\right), \quad t \gg \tau_{\text{m}}, \tau_{\text{im}}, \quad (6)$$

with  $D_{\text{eff}} = D/(1 + \tau_{\text{im}}/\tau_{\text{m}})$ . Note that for asymptotic equalities we use the  $\sim$  symbol. In fact, independent of the ratio  $f_{\text{m}}$  and  $f_{\text{im}}$  we asymptotically obtain a Gaussian

distribution in which the diffusivity is reduced to the effective diffusivity  $D_{\text{eff}}$ . The mobile and immobile concentrations are asymptotically equivalent to (6) up to a scalar  $f_j^{\text{eq}}$  defined below [10].

## 2.2. Moments

In general, the fractions  $\bar{n}_m$  and  $\bar{n}_{\text{im}}$  of mobile and immobile tracers, initially fixed as  $f_m$  and  $f_{\text{im}}$ , change over time. To obtain the respective numbers, we integrate the tracer densities over space. This corresponds to setting  $k = 0$  in the Fourier-Laplace transforms  $n_m(k, s)$  and  $n_{\text{im}}(k, s)$  of the densities. After Laplace inversion we find

$$\bar{n}_m(t) = \frac{\tau_m}{\tau_m + \tau_{\text{im}}} + \frac{f_m \tau_{\text{im}} - f_{\text{im}} \tau_m}{\tau_m + \tau_{\text{im}}} \exp(-[\tau_m^{-1} + \tau_{\text{im}}^{-1}]t), \quad (7)$$

$$\bar{n}_{\text{im}}(t) = \frac{\tau_{\text{im}}}{\tau_m + \tau_{\text{im}}} - \frac{f_m \tau_{\text{im}} - f_{\text{im}} \tau_m}{\tau_m + \tau_{\text{im}}} \exp(-[\tau_m^{-1} + \tau_{\text{im}}^{-1}]t), \quad (8)$$

with  $\bar{n}_m(t) + \bar{n}_{\text{im}}(t) = 1$ . In the long-time limit  $t \gg \tau_m, \tau_{\text{im}}$  the fractions of mobile and immobile tracers reach the stationary values  $f_m^{\text{eq}} = \tau_m / (\tau_m + \tau_{\text{im}})$  and  $f_{\text{im}}^{\text{eq}} = \tau_{\text{im}} / (\tau_m + \tau_{\text{im}})$ , respectively. Our approach of splitting the total concentration into mobile and immobile fractions allows us to calculate the moments of the unbound, bound, and total tau protein distributions individually,

$$\langle x^2(t) \rangle_j = \frac{1}{\bar{n}_j(t)} \int_{-\infty}^{\infty} x^2 n_j(x, t) dx, \quad (9)$$

where  $j$  stands for m, im, and tot [10]. To shorten the notation, we use  $\langle x^2(t) \rangle = \langle x^2(t) \rangle_{\text{tot}}$  in the remainder of this work. Using the Laplace inversion of

$$\left. \frac{\partial^2}{\partial k^2} n_{\text{tot}}(k, s) \right|_{k=0} = \langle x^2(s) \rangle, \quad (10)$$

we obtain the expression

$$\langle x^2(t) \rangle = 2D_{\text{eff}}t + 2D\tau_{\text{im}} \frac{f_m \tau_{\text{im}} / \tau_m - f_{\text{im}}}{(1 + \tau_{\text{im}} / \tau_m)^2} \left( 1 - e^{-(\tau_m^{-1} + \tau_{\text{im}}^{-1})t} \right) \quad (11)$$

for the second moment. In the next section we consider the initial conditions, when all tracers are initially mobile. This is chosen for didactic purposes, as this initial condition shows the plateau in the MSD and intermittent Laplace distribution most clearly. In section 4 we consider immobile initial conditions and finally consider equilibrium initial conditions in section 5, where the effects discussed in earlier sections are present at the same time.

## 3. All tracers initially mobile

We now consider the initial condition when all tracers are mobile, i.e.,  $n_m(x, 0) = \delta(x)$  and  $n_{\text{im}}(x, 0) = 0$ . This initial condition does not correspond to the experiment carried out by [11]. However, this situation could be realised experimentally, e.g., by using the method of injection of fluorescently labelled tau proteins [42]. In what follows we repeatedly use the time scale separation  $\tau_m \ll \tau_{\text{im}}$  observed for tau proteins and also relevant to other systems.

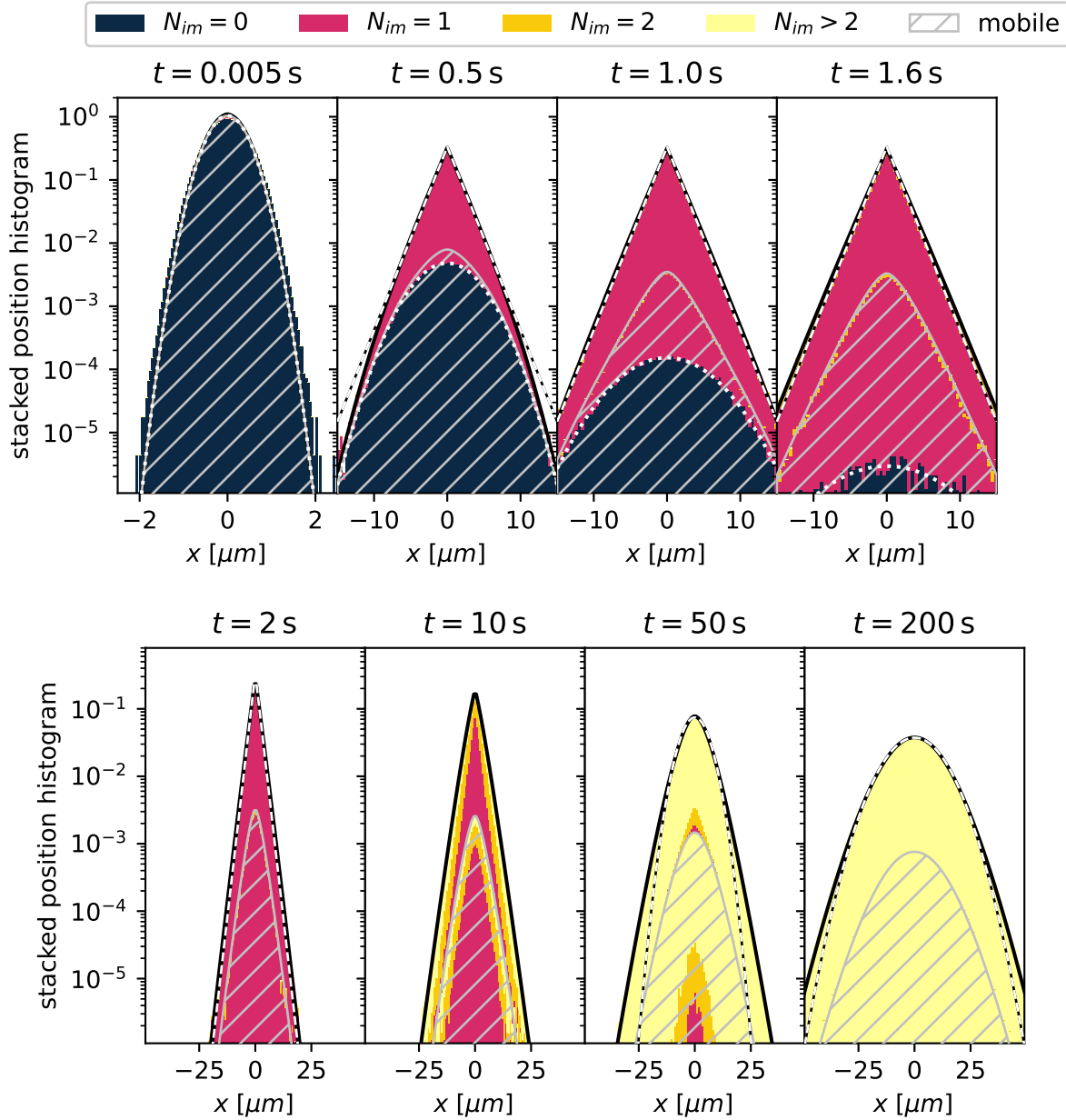


**Figure 2.** Concentration profiles for mobile initial conditions. The solid black line shows  $n_{tot}(x, t)$ , the grey striped area  $n_m(x, t)$  obtained via Laplace inversion of relations (3) and (5). Colours indicate the number of immobilisation events of particles from a Brownian dynamics simulation with  $5 \times 10^6$  trajectories in a stacked histogram. The striped area denotes mobile particles and the white dotted line denotes initially mobile tracers that have not yet been immobilised up to the indicated time  $t$  (13); this result almost coincides with the full concentration in the top left panel. For  $t = 0.5$  sec to 2 sec the white dashed line shows the Laplacian (16), and for  $t = 50$  sec and 200 sec it shows the long-time Gaussian (6).

### 3.1. Concentration

We calculate the densities at short, intermediate and long times. In [Appendix B.1](#) we obtain the Gaussian

$$n_{\text{tot}}(x, t) \sim \frac{1}{\sqrt{4\pi Dt}} \exp\left(-\frac{x^2}{4Dt}\right) \quad (12)$$

in the short time limit  $t \ll \tau_m, \tau_{\text{im}}$ . The Gaussian (12) can be seen in figure 2 in the top left panel. In this figure  $n_m(x, t)$ ,  $n_{\text{tot}}(x, t)$ , and a histogram are shown. The densities are obtained from Laplace inversions of the expressions in Laplace space (5), while the histogram is obtained from simulations, and colours denote the number of immobilisation events  $N_{\text{im}}$ . Initially, all particles are mobile and diffuse freely, as denoted by the black colouring.

The concentration of freely diffusing particles that have not immobilised yet, i.e., have zero immobilisation events  $N_{\text{im}} = 0$ , is given by the PDF of free Brownian motion multiplied by the probability of not having immobilised, i.e.,

$$n_m(x, t | N_{\text{im}} = 0) = \frac{\exp(-t/\tau_m)}{\sqrt{4\pi Dt}} \exp\left(-\frac{x^2}{4Dt}\right). \quad (13)$$

These mobile tracers immobilise with the position dependent rate  $n_m(x, t | N_{\text{im}} = 0)/\tau_m$ . Integrating from  $t' = 0$  to  $t' = t$ , we obtain in the limit  $t \ll \tau_{\text{im}}$  (i.e., at short and intermediate times) that

$$\begin{aligned} n_{\text{im}}(x, t \ll \tau_{\text{im}}) &\sim \int_0^t \frac{\exp(-t'/\tau_m)/\tau_m}{\sqrt{4\pi Dt'}} \exp\left(-\frac{x^2}{4Dt'}\right) dt' \\ &= \frac{\exp(-|x|/\sqrt{D\tau_m})}{\sqrt{4D\tau_m}} \frac{1 - \operatorname{erf}\left(|x|/\sqrt{4Dt} - \sqrt{t/\tau_m}\right)}{2} \\ &\quad - \frac{\exp(|x|/\sqrt{D\tau_m})}{\sqrt{4D\tau_m}} \frac{1 - \operatorname{erf}\left(|x|/\sqrt{4Dt} + \sqrt{t/\tau_m}\right)}{2}. \end{aligned} \quad (14)$$

Comparing (14) with the Laplace inversion of  $n_{\text{im}}(x, s)$  (5) in figure A1 we find very good agreement in the relevant range  $t \ll \tau_{\text{im}}$  §. For the total density we obtain by adding  $n_m(x, t)$  (12) and  $n_{\text{im}}(x, t)$  (14)

$$n_{\text{tot}}(x, t) \sim \frac{\exp(-t/\tau_m)}{\sqrt{4\pi Dt}} \exp\left(-\frac{x^2}{4Dt}\right) + n_{\text{im}}(x, t \ll \tau_{\text{im}}), \quad t \ll \tau_{\text{im}} \quad (15)$$

for the full tracer density. For  $t \ll \tau_m$  we recover the Gaussian (12) from (15), while for  $\tau_m \ll t \ll \tau_{\text{im}}$  the distribution is distinctly non-Gaussian, as shown in figure 2. Up to around  $t = 0.6$  sec, the motion of the free tracers is dominated by the Gaussian  $n_m(x, t | N_{\text{im}} = 0)$ , see (13), which spreads like free Brownian particles, shown as a white dotted line in figure 2. At around  $t = 1.6$  sec, most of the tracers with  $N_{\text{im}} = 0$  immobilised and the majority of mobile tracers were immobile exactly once ( $N_{\text{im}} = 1$ ) and transitioned back to the mobile zone, as shown by the red area. Due to the

§ Equations (13) and (14) can also be obtained by taking the limit  $\tau_{\text{im}} \rightarrow \infty$  in (2) and solving the equations directly.



immobilisation, these tracers have moved less than the free particles with  $N_{\text{im}} = 0$  and a Laplace distribution emerges in the centre. For  $x \ll t\sqrt{D/\tau_m}$  and  $t \gg \tau_m$  we can use the asymptotic  $\lim_{x \rightarrow \infty} \text{erf}(x) = -\lim_{x \rightarrow \infty} \text{erf}(-x) = 1$  in  $n_{\text{im}}(x, t \ll \tau_{\text{im}})$ , equation (14), and obtain from  $n_{\text{tot}}(x, t)$  (15) the expression

$$n_{\text{tot}}(x, t) \sim \frac{1}{\sqrt{4D\tau_m}} \exp\left(-\frac{|x|}{\sqrt{D\tau_m}}\right), \quad (16)$$

in the intermediate time regime  $\tau_m \ll t \ll \tau_{\text{im}}$ . Combining the conditions  $t \ll \tau_m$  and  $x \ll t\sqrt{D/\tau_m}$  leads to  $x \ll \tau_{\text{im}}\sqrt{D/\tau_m} = 71 \mu\text{m}$ , which is large compared to the standard deviation  $\sqrt{2D\tau_m} = 2.1 \mu\text{m}$  of the Laplace distribution (16). This means that the distribution follows such a Laplace shape for a large range of positions. The total concentration, in turn, therefore follows a Laplace distribution with fixed parameters. This is a pronounced deviation from a Gaussian distribution. This result can also be obtained from calculations in Laplace space, as shown in [Appendix B.2](#). In contrast, for times significantly longer than  $\tau_{\text{im}}$ , many immobilisations take place, as shown by the bright yellow area in [figure 2](#), where the distribution follows the Gaussian (6) with the effective diffusivity  $D_{\text{eff}} = D/(1 + \tau_{\text{im}}/\tau_m)$ .

### 3.2. Mean squared displacement

From the general expression for the MSD (11) for immobile initial conditions, we obtain the expression

$$\langle x^2(t) \rangle = \frac{2D}{1 + \tau_{\text{im}}/\tau_m} \left[ t + \frac{\tau_{\text{im}}^2/\tau_m}{1 + \tau_{\text{im}}/\tau_m} \left( 1 - e^{-(\tau_m^{-1} + \tau_{\text{im}}^{-1})t} \right) \right]. \quad (17)$$

At intermediate times the MSD, expression (17), exhibits a plateau-like behaviour with the constant MSD

$$\langle x^2(t) \rangle \sim 2D\tau_m, \quad \tau_m \ll t \ll \tau_{\text{im}}, \quad (18)$$

corresponding to free Brownian particles that moved for the duration  $\tau_m$ . This requires the condition  $\tau_m \ll \tau_{\text{im}}$ , which is satisfied in the tau protein case [11], with  $\tau_m = 0.16$  sec and  $\tau_{\text{im}} = 7.7$  sec. Such plateaus are often found when tracers diffuse in porous media or for dynamics in crowded membranes or environments with obstacles, in which the tracer can be transiently confined [27, 35, 37, 43, 44]. The MSD (17) is shown in [figure 3\(a\)](#) as the black solid line.

When calculating the moments of the mobile and immobile tracers (9), the time-dependent normalisations of the tracer densities (8),

$$\bar{n}_m(t) = \frac{\tau_{\text{im}}}{\tau_m + \tau_{\text{im}}} \left[ 1 + \tau_{\text{im}}/\tau_m e^{-(\tau_m^{-1} + \tau_{\text{im}}^{-1})t} \right] \quad (19)$$

$$\bar{n}_{\text{im}}(t) = \frac{\tau_{\text{im}}}{\tau_m + \tau_{\text{im}}} \left[ 1 - e^{-(\tau_m^{-1} + \tau_{\text{im}}^{-1})t} \right], \quad (20)$$

need to be taken into account, yielding the moments of the mobile and immobile densities (9) [10]

$$\langle x^2(t) \rangle_m = \frac{2D}{(1 + \tau_{\text{im}}/\tau_m)(1 + \tau_{\text{im}}/\tau_m e^{-(\tau_m^{-1} + \tau_{\text{im}}^{-1})t})} \left[ t \left( 1 + \frac{\tau_{\text{im}}^2}{\tau_m^2} e^{-(\tau_m^{-1} + \tau_{\text{im}}^{-1})t} \right) \right]$$

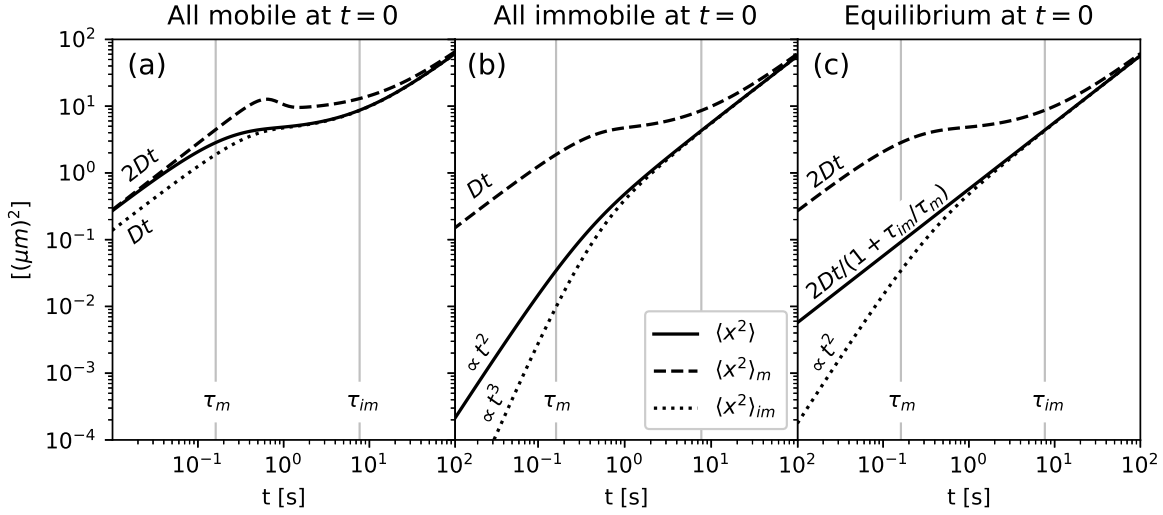


**Figure 3.** Second moments for different initial conditions on a log-log scale. In panel (a) all tracers are initially mobile, as in section 3. After a linear growth, the second moment  $\langle x^2(t) \rangle$  of all tracers, equation (17), shows a plateau for  $\tau_m \ll t \ll \tau_{im}$ . The second moment of the mobile particles, equation (21), in panel (a) has a peak immediately before the total particle moment and the mobile particle moment reach a plateau value. Immobile tracers spread  $\sim Dt$  at short times, and the second moment (22) has a plateau at intermediate times. In panel (b), all tracers are initially immobile, as in section 4. The second moment of all tracers, equation (26), grows  $\sim Dt^2/\tau_{im}$  at short times, due to the decaying number of particles located at  $x = 0$ . The immobile tracers spread  $\sim Dt^3/(3\tau_m\tau_{im})$  at short times, while the full expression is given in equation (26). The mobile tracers in (b) spread exactly like the immobile tracers in (a), where all tracers are initially mobile. Panel (c) shows the equilibrium case, section 5, in which the second moment grows like  $2Dt/(1 + \tau_{im}/\tau_m)$ , equation (35) for all times. The mobile and immobile moments exactly match the moments of the total distribution with mobile and immobile initial conditions, respectively.

$$+ \frac{2\tau_{im}^2/\tau_m}{1 + \tau_{im}/\tau_m} (1 - e^{-(\tau_m^{-1} + \tau_{im}^{-1})t}) \quad (21)$$

and

$$\begin{aligned} \langle x^2(t) \rangle_{im} = & \frac{2D}{1 - e^{-(\tau_m^{-1} + \tau_{im}^{-1})t}} \left[ \frac{t}{1 + \tau_{im}/\tau_m} \left( 1 - \frac{\tau_{im}}{\tau_m} e^{-(\tau_m^{-1} + \tau_{im}^{-1})t} \right) \right. \\ & \left. + \frac{\tau_{im}^2/\tau_m - \tau_{im}}{(1 + \tau_{im}/\tau_m)^2} \left( 1 - e^{-(\tau_m^{-1} + \tau_{im}^{-1})t} \right) \right]. \quad (22) \end{aligned}$$

As shown in figure 3, the mobile second moment exhibits a peak at around  $t = 0.6$  sec, followed by a plateau. This peak arises as the density of mobile tracers initially consists of mobile tracers that have never immobilised. Once  $t \gg \tau_m$  the mobile density mainly consists of tracers that were immobile (at least) once and mobilised, as discussed above. Since the latter had less time to move, they have spread less and the MSD temporarily decreases.

The immobile MSD (22) has the short-time behaviour  $\langle x^2(t) \rangle_{im} \sim Dt$  for  $t \ll \tau_m, \tau_{im}$ . The factor  $\frac{1}{2}$  as compared to the mobile tracers arises because immobile tracers

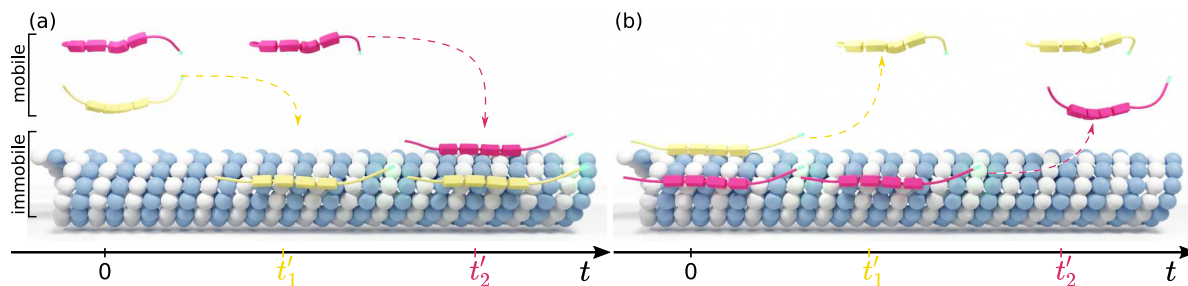


**Figure 4.** Schematic showing the short-time behaviour of tracers for mobile (a) and immobile initial conditions (b) at three snapshots of time. In both panels, the tracers change the mobilisation state at times  $t'_1$  and  $t'_2$ , respectively. For mobile initial conditions in (a), the number of immobile tracers grows  $\sim t/\tau_m$  at short times. Namely, the later a tracer immobilises, the longer it was previously mobile. In (b) the number of mobile tracers grows  $\sim t/\tau_{im}$ . Namely, the earlier a tracer mobilises in (b), the longer it is mobile.

effectively average over the history of the mobile tracers. Namely, for  $t' \ll \tau_m, \tau_{im}$ , mobile particles immobilise with the constant rate  $p(t') = 1/\tau_m$ . A particle that immobilised at time  $t'$  before moved for the duration  $t'$  and thus contributes  $2Dt'$  to the second moment for  $t > t'$ , see figure 4(a) for a schematic drawing. When averaging over different mobile periods  $t'$  and normalising with the fraction of immobile tracers  $\int_0^t p(t')dt'$ , we obtain

$$\langle x^2(t) \rangle_{im} \sim 2D \frac{\int_0^t t' p(t') dt'}{\int_0^t p(t') dt'} = \frac{2D \int_0^t t'/\tau_m dt'}{t/\tau_m} = Dt, \text{ for } t \ll \tau_m, \tau_{im}. \quad (23)$$

As mentioned above, the long-time limits of the MSDs of all densities remain equal to  $2D_{eff}t$ , regardless of the fractions  $f_m$  and  $f_{im}$ .

#### 4. All tracers initially immobile

We now discuss the case when all tracers are immobile at  $t = 0$ ,  $n_{im}(x, 0) = \delta(x)$  and  $n_m(x, 0) = 0$ .

##### 4.1. Concentration

In [Appendix B.1](#), we obtain the short-time behaviour

$$n_{tot}(x, t) \sim \frac{2t/\tau_{im}}{\sqrt{4\pi Dt}} e^{-\frac{x^2}{4Dt}} - \frac{|x|(1 - \text{erf}(\frac{|x|}{\sqrt{4Dt}}))}{2D\tau_{im}} + \left(1 - \frac{t}{\tau_{im}}\right) \delta(x), \text{ for } t \ll \tau_m, \tau_{im} \quad (24)$$

by applying approximations for large  $s$  in Laplace space. Expression (24) is shown in the left panel of figure 5 as the black dashed line. In particular note the distinctively non-Gaussian shape of the distribution in contrast to the case of mobile initial conditions. The Gaussian in equation (24) has the normalisation  $\sim 2t/\tau_{im}$ , while the second term

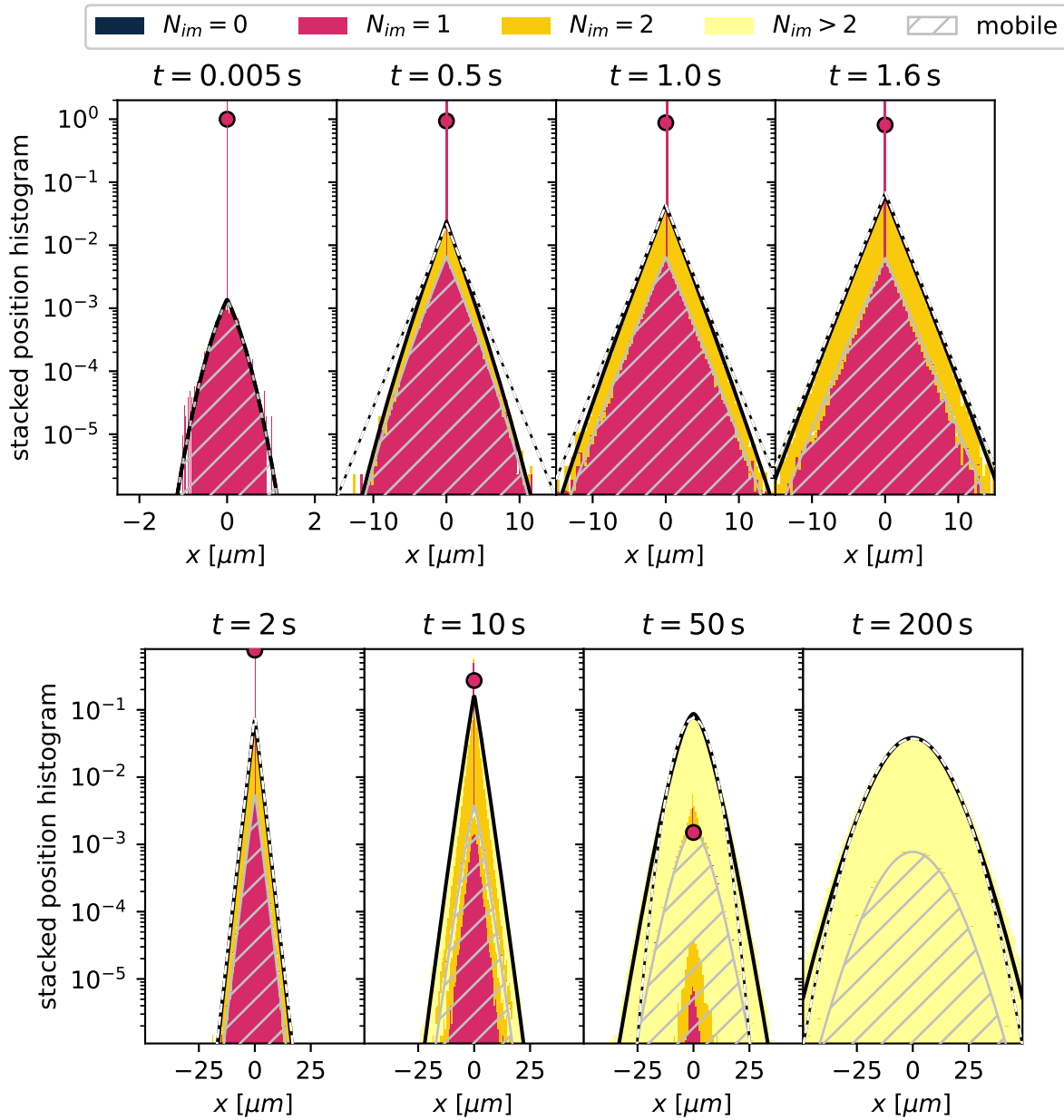


**Figure 5.** Concentration profiles for immobile initial conditions, for a description of the legend see figure 2. The main difference to the case of mobile initial conditions poses the peak of immobile tracers at  $x = 0$  that have not moved up to time  $t$ , as shown by the circle. In addition we here find a pronounced relative increase of mobile particle numbers and the very slow spread of immobile tracers at short times. The short time approximation (24) is shown as the black dashed line in the top left panel. For  $t = 0.5$  sec to 10 sec the white dashed line shows the Laplacian (25) with growing weight, and for  $t = 50$  sec and 200 sec it shows the long-time Gaussian (6).

has the normalisation  $\sim -t/\tau_{\text{im}}$ , and thus the whole expression (24) is normalised to unity. In Appendix B.2 we obtain the total density at intermediate times  $\tau_{\text{m}} \ll t \ll \tau_{\text{im}}$

$$n_{\text{tot}}(x, t) \sim \frac{t/\tau_{\text{im}}}{\sqrt{4D\tau_{\text{m}}}} \exp\left(-\frac{|x|}{\sqrt{D\tau_{\text{m}}}}\right) + \left(1 - \frac{t}{\tau_{\text{im}}}\right) \delta(x), \quad (25)$$

as shown in figure 5 in the top row (except for the leftmost panel) as a black-white striped line. Compared to the mobile initial condition, the coefficient of the Laplace distribution has the linear growth  $t/\tau_{\text{im}}$ . Most tracers remain immobile at the origin at  $t = 1.6$  sec. In Appendix B.4 we find expression (B.11) for  $n_{\text{tot}}(x, t)$ , that is valid for  $t \ll \tau_{\text{im}}$  and contains equations (24) and (25) as limits. In figure 5 the lower panels show the transition from the Laplace distribution to the Gaussian (6).

#### 4.2. Mean squared displacement

From the general expression for the MSD (11), we obtain the expression

$$\langle x^2(t) \rangle = \frac{2D}{1 + \tau_{\text{im}}/\tau_{\text{m}}} \left[ t - \frac{\tau_{\text{im}}}{1 + \tau_{\text{im}}/\tau_{\text{m}}} \left( 1 - e^{-(\tau_{\text{m}}^{-1} + \tau_{\text{im}}^{-1})t} \right) \right]. \quad (26)$$

The MSD (26) has the ballistic short-time behaviour

$$\langle x^2(t) \rangle \sim \frac{Dt^2}{\tau_{\text{im}}} + O(t^3), \quad t \ll \tau_{\text{m}}, \tau_{\text{im}}. \quad (27)$$

The Landau symbol  $O(\cdot)$  represents higher order terms. The ballistic behaviour at short times  $t \ll \tau_{\text{im}}$  arises because the fraction  $\exp(-t/\tau_{\text{im}}) \sim 1 - t/\tau_{\text{im}}$  of tracers are immobile at  $x = 0$  and hence do not contribute to the second moment. For  $t' \ll \tau_{\text{m}} \ll \tau_{\text{im}}$ , immobile particles mobilise with the constant rate  $p(t') = 1/\tau_{\text{im}}$ . A particle that mobilised at time  $t'$  moved for the duration  $t - t'$  and thus contributes  $2D(t - t')$  to the second moment for  $t > t'$ , see figure 4(a) for a schematic drawing. When integrating over different mobilisation times  $t'$  we find

$$\langle x^2(t) \rangle \sim 2D \int_0^t (t - t') p(t') dt' = 2D \int_0^t \frac{t - t'}{\tau_{\text{im}}} dt' = D \frac{t^2}{\tau_{\text{im}}}, \quad t \ll \tau_{\text{m}} \ll \tau_{\text{im}}. \quad (28)$$

We obtain the number of free and bound tracers from the general expression (8),

$$\bar{n}_{\text{m}}(t) = \frac{\tau_{\text{m}}}{\tau_{\text{m}} + \tau_{\text{im}}} \left[ 1 - e^{-(\tau_{\text{m}}^{-1} + \tau_{\text{im}}^{-1})t} \right] \quad (29)$$

$$\bar{n}_{\text{im}}(t) = \frac{\tau_{\text{im}}}{\tau_{\text{m}} + \tau_{\text{im}}} \left[ 1 + \tau_{\text{m}}/\tau_{\text{im}} e^{-(\tau_{\text{m}}^{-1} + \tau_{\text{im}}^{-1})t} \right]. \quad (30)$$

This produces the normalisation of the immobile moment, and we find

$$\langle x^2(t) \rangle_{\text{im}} = \frac{2Dt}{1 + \tau_{\text{m}}/\tau_{\text{im}}} \frac{1 + e^{-(\tau_{\text{m}}^{-1} + \tau_{\text{im}}^{-1})t}}{\tau_{\text{im}}/\tau_{\text{m}} + e^{-(\tau_{\text{m}}^{-1} + \tau_{\text{im}}^{-1})t}} - \frac{4D\tau_{\text{im}}^2/\tau_{\text{m}}}{(1 + \tau_{\text{im}}/\tau_{\text{m}})^2} \frac{1 - e^{-(\tau_{\text{m}}^{-1} + \tau_{\text{im}}^{-1})t}}{\tau_{\text{im}}/\tau_{\text{m}} + e^{-(\tau_{\text{m}}^{-1} + \tau_{\text{im}}^{-1})t}}. \quad (31)$$

This MSD has the short-time behaviour  $\langle x^2(t) \rangle_{\text{im}} \sim Dt^3/(3\tau_{\text{im}}\tau_{\text{m}})$  for  $t \ll \tau_{\text{m}}, \tau_{\text{im}}$ . The cubic scaling emerges as the only immobile tracers, that are not located at the origin, have previously mobilised and then immobilised again. The mobile concentration grows

$\sim t/\tau_{\text{im}}$  at short times  $t \ll \tau_{\text{im}}$ . Integrating over the time  $t'$  spent in the mobile phase yields the cubic scaling

$$\langle x^2(t) \rangle_{\text{im}} \sim 2D \int_0^t \frac{1}{\tau_{\text{m}}} n_{\text{m}}(t-t') t' dt' = \frac{2D}{\tau_{\text{m}} \tau_{\text{im}}} \int_0^t (t-t') t' dt' = D \frac{t^3}{3\tau_{\text{m}} \tau_{\text{im}}}, \quad (32)$$

where in the first step we took the limit  $t \ll \tau_{\text{m}}$ . Since the mobile concentration with immobile initial conditions is proportional to the immobile concentration with mobile initial conditions,  $\langle x^2(t) \rangle_{\text{m}}$  is equal to  $\langle x^2(t) \rangle_{\text{im}}$  in (22) with mobile initial conditions. This can be seen in figure 3(a) and 3(b). As for the mobile initial condition considered in section 3, the MSDs of all densities grow  $\sim 2D_{\text{eff}}t$  asymptotically.

## 5. Equilibrium initial fractions of initial mobile tracers

In this section we use the equilibrium values  $n_{\text{m}}(x, 0) = f_{\text{m}}^{\text{eq}}\delta(x)$  and  $n_{\text{im}}(x, 0) = f_{\text{im}}^{\text{eq}}\delta(x)$  as initial conditions.

### 5.1. Concentration profiles

From the general expressions (3) and (5) for the densities  $n_{\text{m}}(x, s)$  and  $n_{\text{tot}}(x, s)$  we find that the mobile concentration of the equilibrium case discussed here is proportional to the total concentration for the mobile initial condition in section 3 at all times. To understand why this is true, we notice that both concentrations at all times contain mobile tracers that were initially mobile. Moreover, from equations (3) and (5) we see that the mobile concentration of the equilibrium case contains initially immobile tracers, while the total concentration contains immobile tracers, that were initially mobile. In equations (3) and (5) the respective terms, that appear in addition to the initially mobile fractions that are still mobile are proportional to each other at all times, as described in section 2.1. An analogous relation holds between the immobile concentration with equilibrium initial conditions and the total concentration with immobile initial conditions, as can be seen in equations (3) and (5).

We consider the short-time approximation  $t \ll \tau_{\text{m}}, \tau_{\text{im}}$  for which initially immobile tracers have not yet mobilised and initially mobile tracers have not yet been trapped. Therefore, we can neglect the terms with the rates  $\tau_{\text{m}}^{-1}$  and  $\tau_{\text{im}}^{-1}$  in (2) and solve  $n_{\text{m}}(x, t)$  and  $n_{\text{im}}(x, t)$  separately, yielding

$$n_{\text{tot}}(x, t) \sim \frac{f_{\text{m}}^{\text{eq}}}{\sqrt{4\pi Dt}} \exp\left(-\frac{x^2}{4Dt}\right) + f_{\text{im}}^{\text{eq}}\delta(x), \quad t \ll \tau_{\text{m}}, \tau_{\text{im}}, \quad (33)$$

with a Gaussian distribution describing free diffusion in addition to a Dirac- $\delta$  distribution of initially immobile tracers that have not yet moved. This behaviour can be seen in the top left panel of figure 6. The same result as (33) can be obtained by combining the short-time expressions for the mobile (12) and immobile (24) initial conditions for  $t \ll \tau_{\text{m}}, \tau_{\text{im}}$ , as done in equation (B.5). At short times, the total density

(33) behaves like the case of mobile initial conditions with an additional delta peak. At intermediate times  $\tau_m \ll t \ll \tau_{im}$  we obtain

$$n_{\text{tot}}(x, t) \sim \frac{t/\tau_{im}}{\sqrt{4D\tau_m}} \exp\left(-\frac{|x|}{\sqrt{D\tau_m}}\right) + \left(1 - \frac{t}{\tau_{im}}\right) \delta(x) \quad (34)$$

by combining the mobile (16) and immobile expression (25), respectively<sup>||</sup>. In fact equation (34) is the same as expression (25) for the case of immobile initial conditions, in the intermediate time regime. This result is shown in figure 6 where this approximation is compared to the full concentration from  $t = 0.5$  to  $t = 2$ . This result is the one-dimensional equivalent to the findings in [21]. The lower right panels of figure 6 show the Gaussian long-time limit (6) as a black-white striped line.

### 5.2. Mean squared displacement

The number of mobile and immobile tracers remains constant for equilibrium initial conditions. At all times the second moment of all tracers (11) thus simplifies to

$$\langle x^2(t) \rangle = \frac{2D}{1 + \tau_{im}/\tau_m} t. \quad (35)$$

The second moment is similar to that of a free Brownian particle, with the effective diffusion coefficient  $D_{\text{eff}} = D/(1 + \tau_{im}/\tau_m)$ , as shown in figure 3. This is a known result from models for Fickian yet non-Gaussian diffusion [21]. The mobile and immobile moments,  $\langle x^2(t) \rangle_m$  and  $\langle x^2(t) \rangle_{im}$  are equivalent to the moments of the full density with mobile (17) and immobile (26) initial conditions, as can be seen in figure 3. This relation holds because the respective densities are proportional, as discussed above. The mobile and immobile moments show clear anomalous diffusion for  $t \ll \tau_{im}$ , with a quite long crossover dynamics, as depicted in figure 3c. The mobile moment has a plateau in the intermediate regime  $\tau_m \ll t \ll \tau_{im}$  and the immobile moment behaves ballistically at short times  $t \ll \tau_m$ .

In the long-time limit all mobile and immobile second moments grow like the moments of the total concentration, i.e.,  $\langle x^2(t) \rangle_m \sim \langle x^2(t) \rangle_{im} \sim 2D_{\text{eff}}t$  for  $t \gg \tau_{im}, \tau_m$ .

## 6. Conclusion

We considered a quite simple mobile-immobile model according to which tracer particles switch between a mobile diffusing state and an immobilised state. On average, the tracers remain mobile for the duration  $\tau_m$  and immobile for  $\tau_{im}$ . We considered the particular case, motivated by experiments on tau proteins binding to and unbinding from microtubules in axons of dendritic cells [11], when the two timescales are separated  $\tau_m \ll \tau_{im}$ . We analysed three different initial conditions with varying fractions of mobile to immobile tracers at the origin, that can, in principle, all be realised in experiments.

<sup>||</sup> An approximation for the whole range of  $t \ll \tau_{im}$  can be obtained for any fractions of initially mobile tracers  $f_m$  by combining equations (15) and (B.11) from the mobile and immobile initial conditions, respectively. This yields equation (B.12) and is shown in figure B2.

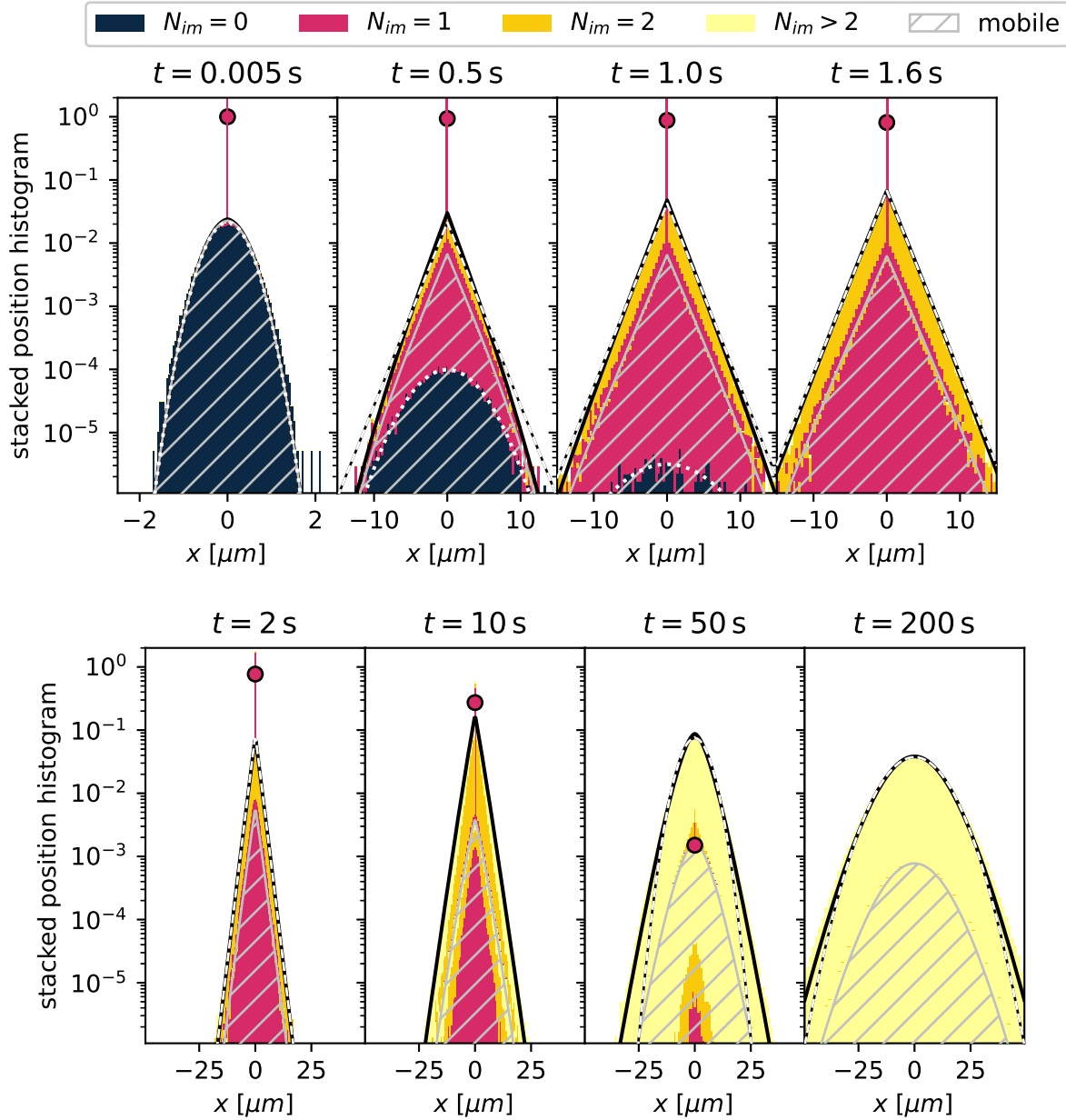


**Figure 6.** Concentration profiles for equilibrium initial conditions. At  $t = 0$  all tracers are at  $x = 0$  and the equilibrium fraction  $\tau_{im}/(\tau_m + \tau_{im})$  is immobile. For a description of the legend see figure 2. The top left panel shows the short-time behaviour consisting of a Gaussian and a  $\delta$ -distribution, equation (33). At  $t = 1$  almost all initially mobile tracers immobilised at least once and the total concentration follows the Laplace distribution (34), as shown by the black-white striped line for  $t = 0.5$ sec to 2sec. At longer times, after several immobilisations the concentration profiles cross over to a Gaussian, as witnessed by equation (6), shown as a black-white striped line for  $t = 50$ sec and  $t = 200$ sec.



First, we studied the case when all tracers are initially mobile, as described in the experiment in [42]. Second, we assumed all tracers to be initially immobile. Third, we considered an equilibrium fraction, corresponding to the experiment in [11]. For non-equilibrium fractions of initially mobile tracers we find anomalous diffusion at short and intermediate timescales, at which initially mobile tracers display a plateau in the MSD at intermediate times and initially immobile tracers spread ballistically at short times. At  $t \ll \tau_m$  and an initial equilibrium fraction, the tracer density consists of a Gaussian and a delta peak. Initially mobile tracers follow a Gaussian distribution at short times. When all tracers are initially immobile, the short time distribution consists of a delta peak and a non-Gaussian distribution. At intermediate times  $\tau_m \ll t \ll \tau_{im}$  the distribution is made up of a Laplace distribution and a delta distribution of initially immobile tracers that have not moved yet. The coefficients of the two distributions depend on the specific initial conditions. We additionally obtain expressions for the densities that are valid for the whole range  $t \ll \tau_{im}$ . We stress that the distribution is non-Gaussian at intermediate times, regardless of the initial conditions. In contrast, the distribution asymptotically at long times matches a Gaussian for all initial conditions. The densities of mobile and immobile tracers with equilibrium initial conditions match the total tracer densities of mobile and immobile initial conditions, respectively, at all times. Moreover, the immobile tracer density from mobile initial conditions is proportional to the mobile tracer density from immobile initial conditions at all times. As a special case for equilibrium initial conditions, our model corresponds to the one-dimensional version of the model used in [21] to describe Fickian yet non-Gaussian diffusion. We find the same linear MSD for all times and obtain a closed expression for the Laplace distribution at intermediate timescales.

The model developed here is, of course, much more general. We provided the framework for any ratio of the characteristic time scales  $\tau_m$  and  $\tau_{im}$ , such that the model will be useful for scenarios ranging from geophysical experiments with Poissonian (im)mobilisation statistics, to molecular systems such as protein (un)binding to DNA in nanochannel setups. It will be a topic of future research to study the effect of a drift velocity in the mobile phase, as well as what happens when non-exponential (im)mobilisation is considered.

## Acknowledgments

We acknowledge funding from the German Science Foundation (DFG, grant no. ME 1535/12-1). AVC acknowledges the support of the Polish National Agency for Academic Exchange (NAWA).

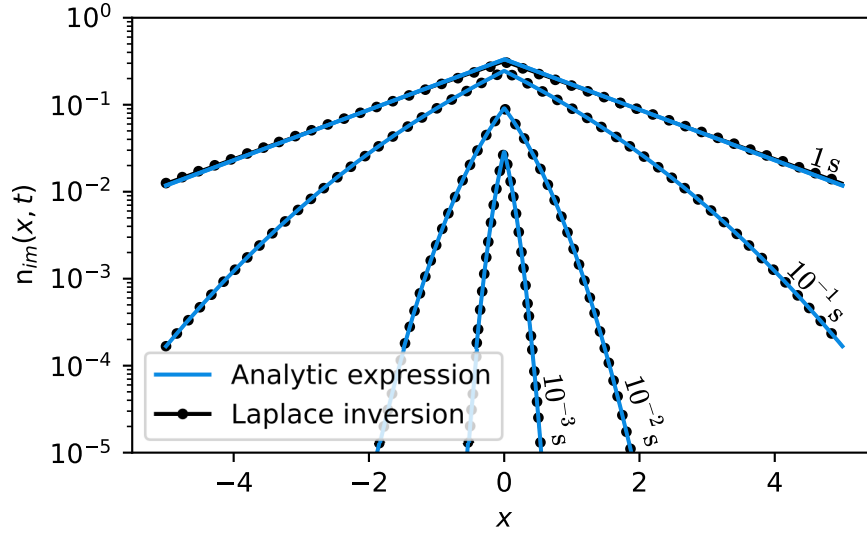


**Figure A1.** Comparison of the Laplace inversion of  $n_{\text{im}}(x, s)$ , expression (5), and the analytic expression for  $n_{\text{im}}(x, t)$ , equation (14), that holds for  $t \ll \tau_{\text{im}}$ . Both overlap almost perfectly for  $t < \tau_{\text{im}} = 7.7$  sec.

## Appendix A. General equations

Starting with equation (2) we apply the Fourier-Laplace transform  $f(k, s) = \int_{-\infty}^{\infty} \int_0^{\infty} e^{-st+ikx} f(x, t) dt dx$  to the rate to obtain

$$n_{\text{m}}(k, s) = \frac{f_{\text{m}} + f_{\text{im}} \frac{1}{1+s\tau_{\text{im}}}}{\phi(s) + k^2 D}$$

$$n_{\text{im}}(k, s) = \frac{\tau_{\text{im}}}{1 + s\tau_{\text{im}}} \left( f_{\text{im}} + \tau_{\text{im}}^{-1} \frac{f_{\text{m}} + f_{\text{im}} \frac{1}{1+s\tau_{\text{im}}}}{\phi(s) + k^2 D} \right) \quad (\text{A.1})$$

as well as

$$n_{\text{tot}}(k, s) = n_{\text{m}}(k, s) + n_{\text{im}}(k, s) = \frac{f_{\text{m}} + f_{\text{im}} \frac{1}{1+s\tau_{\text{im}}}}{s} \frac{\phi(s)}{\phi(s) + k^2 D} + f_{\text{im}} \frac{\tau_{\text{im}}}{1 + s\tau_{\text{im}}} \quad (\text{A.2})$$

with  $\phi(s) = s[1 + \tau_{\text{im}}\tau_{\text{m}}^{-1}/(1 + s\tau_{\text{im}})]$ .

## Appendix B. Asymptotics calculated in Laplace space

We go from short-time limit to long-time limit.

### Appendix B.1. Short-time limit

For  $t \ll \tau_{\text{m}}, \tau_{\text{im}}$ , we obtain  $s\tau_{\text{im}} \gg 1$  and  $s\tau_{\text{m}} \gg 1$ . This yields  $\phi(s) \sim s$  in this limit. With (A.1) for  $f_{\text{m}} = 1$  and  $f_{\text{im}} = 0$  we obtain the expression

$$n_{\text{m}}(k, s) \sim n_{\text{tot}}(k, s) \sim \frac{1}{s + k^2 D} \quad (\text{B.1})$$

which produces the Gaussian (12). We now consider  $f_{\text{im}} = 1$  and  $f_{\text{m}} = 0$  and obtain the expression

$$n_{\text{tot}}(k, s) \sim \frac{1}{s\tau_{\text{im}}} \frac{1}{s + k^2 D} + \left( \frac{1}{s} - \frac{1}{s^2 \tau_{\text{im}}} \right) \quad (\text{B.2})$$

from (A.2) in the limit  $s\tau_{\text{m}} \gg 1$  and  $s\tau_{\text{im}} \gg 1$ . Fourier-Laplace inversion yields the expression

$$n_{\text{tot}}(x, t) \sim \frac{1}{\tau_{\text{im}}} \int_0^t \frac{1}{\sqrt{4\pi D t'}} e^{-\frac{x^2}{4Dt'}} dt' + (1 - t/\tau_{\text{im}}) \delta(x) \quad \text{for } t \ll \tau_{\text{m}} \ll \tau_{\text{im}}. \quad (\text{B.3})$$

Solving the integral in (B.3) gives the expression

$$n_{\text{tot}}(x, t) \sim \frac{2t/\tau_{\text{im}}}{\sqrt{4\pi D t}} e^{-\frac{x^2}{4Dt}} - \frac{|x|(1 - \text{erf}(\frac{|x|}{\sqrt{4Dt}}))}{2D\tau_{\text{im}}} + \left(1 - \frac{t}{\tau_{\text{im}}}\right) \delta(x), \quad \text{for } t \ll \tau_{\text{m}} \ll \tau_{\text{im}}, \quad (\text{B.4})$$

where normalisation is conserved. By combining expression (B.4) for immobile initial conditions and (12) for mobile initial conditions, we obtain the expression

$$n_{\text{tot}}(x, t) \sim (f_{\text{m}} + 2f_{\text{im}}t/\tau_{\text{im}}) \frac{1}{\sqrt{4\pi D t}} e^{-\frac{x^2}{4Dt}} - f_{\text{im}} \frac{|x|(1 - \text{erf}(\frac{|x|}{\sqrt{4Dt}}))}{2D\tau_{\text{im}}} + f_{\text{im}} \left(1 - \frac{t}{\tau_{\text{im}}}\right) \delta(x), \quad (\text{B.5})$$

for  $t \ll \tau_{\text{m}} \ll \tau_{\text{im}}$  for arbitrary fractions of initially mobile tracers.

### Appendix B.2. Density at intermediate timescales

We now investigate the intermediate time  $\tau_{\text{m}} \ll t \ll \tau_{\text{im}}$ , corresponding to  $s\tau_{\text{m}} \ll 1$  and  $s\tau_{\text{im}} \gg 1$ . In this regime we have  $\phi(s) \sim \tau_{\text{m}}^{-1}$ , yielding the expression

$$n_{\text{tot}}(x, s) \sim \frac{f_{\text{m}} + f_{\text{im}} \frac{1}{s\tau_{\text{im}}}}{s} \frac{1}{\sqrt{4D\tau_{\text{m}}}} e^{-\frac{|x|}{\sqrt{D\tau_{\text{m}}}}} + f_{\text{im}} \left( \frac{1}{s} - \frac{1}{s^2 \tau_{\text{im}}} \right) \delta(x). \quad (\text{B.6})$$

from (5) for the total concentration. Inverse Laplace transform of (B.6) yields the expression

$$n_{\text{tot}}(x, t) \sim (f_{\text{m}} + f_{\text{im}}t/\tau_{\text{im}}) \frac{1}{\sqrt{4D\tau_{\text{m}}}} e^{-\frac{|x|}{\sqrt{D\tau_{\text{m}}}}} + f_{\text{im}} (1 - t/\tau_{\text{im}}) \delta(x) \quad (\text{B.7})$$

for  $\tau_{\text{m}} \ll t \ll \tau_{\text{im}}$ .

### Appendix B.3. Density in the long-time limit

We obtain the long-time limit  $t \gg \tau_{\text{m}}, \tau_{\text{im}}$  from  $n_{\text{tot}}(k, s)$  (A.2) using  $s \ll 1/\tau_{\text{im}}, 1/\tau_{\text{m}}$  and  $\phi(s) \sim s(1 + \tau_{\text{im}}/\tau_{\text{m}})$ . This yields the expression

$$n_{\text{tot}}(x, t) \sim \frac{1}{\sqrt{4\pi D_{\text{eff}} t}} e^{-\frac{x^2}{4D_{\text{eff}} t}}, \quad \text{for } t \gg \tau_{\text{m}}, \tau_{\text{im}}, \quad (\text{B.8})$$

with  $D_{\text{eff}} = D/(1 + \tau_{\text{im}}/\tau_{\text{m}})$ .

## Appendix B.4. Density at short to intermediate timescales

Here we analyse the regime  $t \ll \tau_{\text{im}}$ . The case  $f_m = 1$  and  $f_{\text{im}} = 0$  is considered in section 3. We consider the case  $f_{\text{im}} = 1$  and  $f_m = 0$  here. From  $n(x, s)$  (5), we obtain with  $s\tau_{\text{im}} \gg 1$  and  $\phi(s) \sim s + 1/\tau_m$

$$n_{\text{tot}}(x, s) \sim \frac{s\tau_m + 1}{s^2\tau_{\text{im}}\tau_m} \frac{1}{\sqrt{4D(s + 1/\tau_m)}} e^{-\sqrt{\frac{s+1/\tau_m}{D}}|x|} + \left(\frac{1}{s} - \frac{1}{s^2\tau_{\text{im}}}\right), \quad \text{for } s\tau_{\text{im}} \gg 1. \quad (\text{B.9})$$

In time-domain in the limit  $t \ll \tau_{\text{im}}$  this corresponds to the expression

$$\begin{aligned} n_{\text{tot}}(x, t) &\sim \int_0^t \frac{t + \tau_m - t'}{\tau_{\text{im}}\tau_m} \exp(-t'/\tau_m) \frac{\exp\left(-\frac{x^2}{4Dt'}\right)}{\sqrt{4Dt'}} dt' + (1 - t/\tau_{\text{im}})\delta(x) \quad (\text{B.10}) \\ &= \frac{e^{-\frac{x^2}{4Dt}}}{\sqrt{4\pi Dt}} e^{-t/\tau_m} \frac{t}{\tau_{\text{im}}} + (1 - t/\tau_{\text{im}})\delta(x) \\ &+ \frac{\exp(-|x|/\sqrt{D\tau_m})}{\sqrt{4D\tau_m}} \left( t/\tau_{\text{im}} - |x| \sqrt{\frac{\tau_m}{4D\tau_{\text{im}}^2}} + \tau_m/2\tau_{\text{im}} \right) \frac{1 - \text{erf}\left(|x|/\sqrt{4Dt} - \sqrt{t/\tau_m}\right)}{2} \\ &- \frac{\exp(|x|/\sqrt{D\tau_m})}{\sqrt{4D\tau_m}} \left( t/\tau_{\text{im}} + |x| \sqrt{\frac{\tau_m}{4D\tau_{\text{im}}^2}} + \tau_m/2\tau_{\text{im}} \right) \frac{1 - \text{erf}\left(|x|/\sqrt{4Dt} + \sqrt{t/\tau_m}\right)}{2}. \end{aligned} \quad (\text{B.11})$$

Normalisation is preserved, as can be seen by integrating (B.10) over  $x$ . The first summand in (B.10) then resolves to  $t/\tau_{\text{im}}$ . In the limit  $t \ll \tau_m, \tau_{\text{im}}$  we recover the short-time behaviour for  $n_{\text{tot}}(x, t)$  (B.4), as shown in figure B1. For  $\tau_m \ll t \ll \tau_{\text{im}}$  and  $|x| \ll \sqrt{4D\tau_{\text{im}}^2/\tau_m}$  we recover the Laplacian intermediate regime in (B.7) with  $f_{\text{im}} = 1$  and  $f_m = 0$ . In figure B1 we show a verification of (B.11). For arbitrary fractions of initially mobile tracers we combine equation (B.11) for immobile initial conditions with equation (15) for mobile initial conditions, as follows

$$\begin{aligned} n_{\text{tot}}(x, t) &\sim \frac{e^{-\frac{x^2}{4Dt}}}{\sqrt{4\pi Dt}} e^{-t/\tau_m} \left( f_m + f_{\text{im}} \frac{t}{\tau_{\text{im}}} \right) + f_{\text{im}}(1 - t/\tau_{\text{im}})\delta(x) \\ &+ \left[ f_m + f_{\text{im}} \left( t/\tau_{\text{im}} - |x| \sqrt{\frac{\tau_m}{4D\tau_{\text{im}}^2}} + \tau_m/2\tau_{\text{im}} \right) \right] \\ &\times \frac{\exp(-|x|/\sqrt{D\tau_m})}{\sqrt{4D\tau_m}} \frac{1 - \text{erf}\left(|x|/\sqrt{4Dt} - \sqrt{t/\tau_m}\right)}{2} \\ &- \left[ f_m + f_{\text{im}} \left( t/\tau_{\text{im}} + |x| \sqrt{\frac{\tau_m}{4D\tau_{\text{im}}^2}} + \tau_m/2\tau_{\text{im}} \right) \right] \\ &\times \frac{\exp(|x|/\sqrt{D\tau_m})}{\sqrt{4D\tau_m}} \frac{1 - \text{erf}\left(|x|/\sqrt{4Dt} + \sqrt{t/\tau_m}\right)}{2}. \end{aligned} \quad (\text{B.12})$$

In figure B2 expression (B.12) is compared to the Laplace inversion of the exact expression of  $n_{\text{tot}}(x, s)$  (5).

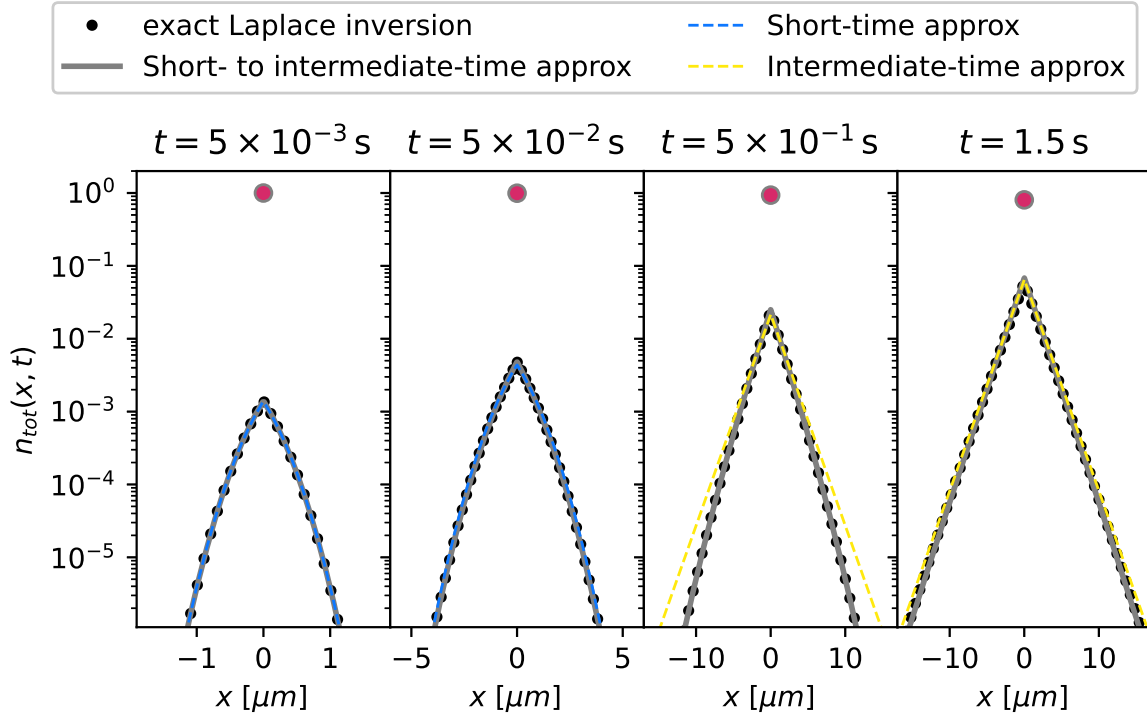


**Figure B1.** All tracers initially immobile. Comparison of the exact Laplace inversion of (5), the short-time approximation (B.4), intermediate time-approximation (B.7) and short to intermediate-time approximation (B.11).

## References

- [1] J. W. Biggar and D. R. Nelson, Miscible displacement and leaching phenomena, in R. M. Hagen, Editor, Irrigation of agricultural lands, *Agronomy* **11**, 254 (1967).
- [2] L. Lapidus and N. R. Amundson, Mathematica of adsorption in beds. VI. The effect of longitudinal diffusion in ion exchange and chromatographic columns, *J. Phys. Chem.* **56**, 984 (1952).
- [3] H. H. Deans, A mathematical model for dispersion in the direction of flow of porous media, *Soc. Pet. Eng. J.* **3**, 49 (1963).
- [4] K. H. Coats and B. D. Smith, Dead-end pore volume and dispersion in porous media, *Soc. Pet. Eng. J.* **4**, 73 (1964).
- [5] M. T. Van Genuchten and P.J. Wierenga, Mass transfer studies in sorbing porous media I. Analytical solutions, *Soil Sci. Soc. Am. J.* **40**, 473 (1976).
- [6] R. Metzler and J. Klafter, The random walk's guide to anomalous diffusion: A fractional dynamics approach, *Phys. Rep.* **339**, 1 (2000).
- [7] J. M. Boggs, S. C. Young, L. M. Beard, L. W. Gelhar, K. R. Rehfeldt, and E. E. Adams, Field study of dispersion in a heterogeneous aquifer: 1. Overview and site description, *Water Res. Res.* **28**, 3281 (1992).
- [8] N. Goepfert, N. Goldscheider, and B. Berkowitz, Experimental and modeling evidence of kilometer-scale anomalous tracer transport in an alpine karst aquifer, *Water Res.* **178**, 115755 (2020).
- [9] R. Schumer, D. A. Benson, M. M. Meerschaert, and B. Baeumer, Fractal mobile/immobile solute transport, *Water Res. Res.* **39**, 13 (2003).
- [10] T. J. Doerries, A. V. Chechkin, R. Schumer, and R. Metzler, Rate equations, spatial moments, and concentration profiles for mobile-immobile models with power-law and mixed waiting time

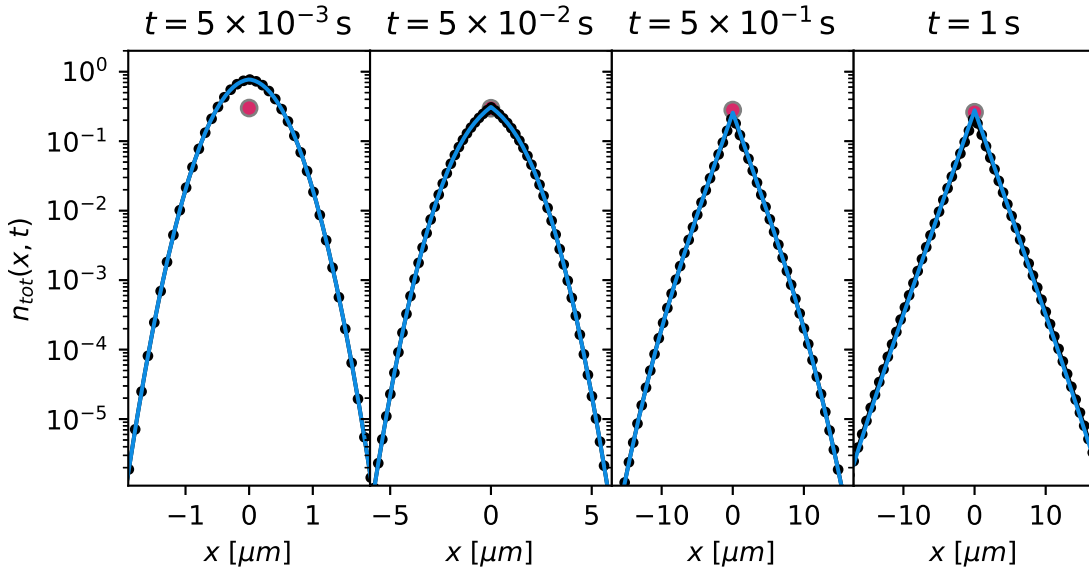


**Figure B2.** Total concentration  $n_{\text{tot}}(x, t)$  for  $f_{\text{im}} = 3/10$  and  $f_{\text{m}} = 7/10$ . Expression (B.12) is shown as blue line and the Laplace inversion of  $n_{\text{tot}}(x, s)$  (5) is shown as black line with markers. Both overlap over five decades in amplitude, for all times shown. The red marker with the grey edge at  $x = 0$  denotes the initially immobile tracers that have not yet moved. At short times the distribution consists of the particles at  $x = 0$  and a Gaussian. At  $t = 1\text{ s}$  the distribution follows a Laplace distribution (linear tails in the log-linear plot), on top of the particles at  $x = 0$ .

distributions, Phys. Rev. E **105**, 014105 (2022).

- [11] M. Igaev, D. Janning, F. Sündermann, B. Niewidok, R. Brandt, and W. Junge, A Refined Reaction-Diffusion Model of Tau-Microtubule Dynamics and its Application in FDAP Analysis, Biophys. J. **107**, 2567 (2014).
- [12] D. Janning, M. Igaev, F. Sündermann, J. Brühmann, O. Beutel, J. J. Heinisch, L. Bakota, J. Piehler, W. Junge, and R. Brandt, Single-molecule tracking of tau reveals fast kiss-and-hop interaction with microtubules in living neurons, Mol. Biol. Cell. **25**, 3541 (2014).
- [13] C. Yeung, M. Shtrahman, and X. L. Wu, Stick-and-diffuse and caged diffusion: a comparison of two models of synaptic vesicle dynamics, Biophys. J. **92**, 2271 (2007).
- [14] B. L. Sprague, R. L. Pego, D. A. Stavreva, and J. G. McNally, Analysis of binding reactions by fluorescence recovery after photobleaching, Biophys. J. **86**, 3473 (2004).
- [15] Z. Liu, W. R. Legant, B. C., Chen, L. Li, J. B. Grimm, L.D. Lavis, E. Betzig, and R. Tjian, 3D imaging of Sox2 enhancer clusters in embryonic stem cells, elife **3**, e04236 (2014).
- [16] D. Mazza, A. Abernathy, N. Golob, T. Morisaki, and J.G. McNally, A benchmark for chromatin binding measurements in live cells, Nucleic Acids Res. **40**, e119 (2012).
- [17] J. Chen, Z. Zhang, L. Li, B. C. Chen, A. Revyakin, B. Hajj, W. Legant, M. Dahan, T. Lionnet, E. Betzig, R. Tjian, and Z. Liu, Single-molecule dynamics of enhanceosome assembly in embryonic stem cells, Cell **156**, 1274 (2014).
- [18] M. M. Wu, E. D. Covington, and R. S. Lewis, Single-molecule analysis of diffusion and trapping of STIM1 and Orail1 at endoplasmic reticulum-plasma membrane junctions, Mol. Biol. Cell **25**, 3672 (2014).
- [19] M. Kolarova, F. García-Sierra, A. Bartos, J. Rieny, and D. Ripova, Structure and pathology of tau protein in Alzheimer disease, J. Alzheimer's Dis. **2012**, 731526 (2012).
- [20] T. Guo, W. Noble, and D. P. Hanger, Roles of tau protein in health and disease, Acta Neuropathol.

- 133**, 665 (2017).
- [21] S. Mora and Y. Pomeau, Brownian diffusion in a dilute field of traps is Fickian but non-Gaussian, *Phys. Rev. E* **98**, 040101 (2018).
- [22] B. Wang, S. M. Anthony, S. C. Bae, and S. Granick, Anomalous yet brownian, *Proc. Natl. Acad. Sci. USA* **106**, 15160 (2009).
- [23] M. J. Skaug, J. Mabry, and D. K. Schwartz, Intermittent Molecular Hopping at the Solid-Liquid Interface, *Phys. Rev. Lett.* **110**, 256101 (2013).
- [24] I. Chakraborty, and Y. Roichman, Disorder-induced Fickian, yet non-Gaussian diffusion in heterogeneous media. *Phys. Rev. Res.* **2**, 022020 (2020).
- [25] A. V. Chechkin, F. Seno, R. Metzler, and I. M. Sokolov, Brownian yet non-Gaussian diffusion: from superstatistics to subordination of diffusing diffusivities, *Phys. Rev. X* **7**, 021002 (2017).
- [26] M. V. Chubynsky and G.W. Slater, Diffusing diffusivity: a model for anomalous, yet Brownian, diffusion, *Phys. Rev. Lett.* **113**, 098302 (2014).
- [27] B. Wang, J. Kuo, S. C. Bae, and S. Granick, When Brownian diffusion is not Gaussian, *Nat. Mater.* **11**, 481 (2012).
- [28] V. Sposini, A. V. Chechkin, F. Seno, G. Pagnini, and R. Metzler, Random diffusivity from stochastic equations: comparison of two models for Brownian yet non-Gaussian diffusion, *New J. Phys.* **20**, 043044 (2018).
- [29] Y. Lanoiselée, and D.S. Grebenkov, A model of non-Gaussian diffusion in heterogeneous media, *J. Phys. A: Math. Theor.* **51**, 145602 (2018).
- [30] R. Jain, and K. L. Sebastian, Diffusion in a crowded, rearranging environment, *J. Phys. Chem. B*, **120**, 3988 (2016).
- [31] M. Javanainen, H. Hammaren, L. Monticelli, J. H. Jeon, R. Metzler, and I. Vattulainen, Anomalous and normal diffusion of proteins and lipids in crowded lipid membranes, *Faraday Discussions* **161**, 397 (2013).
- [32] E. Yamamoto, T. Akimoto, A. Mitsutake, and R. Metzler, Universal relation between instantaneous diffusivity and radius of gyration of proteins in aqueous solution, *Phys. Rev. Lett.* **126**, 128101 (2021).
- [33] F. Baldovin, E. Orlandini, and F. Seno, Polymerization induces non-Gaussian diffusion, *Frontiers Phys.* **7**, 124 (2019).
- [34] M. Hidalgo-Soria and E. Barkai, The hitchhiker model for Laplace diffusion processes in the cell environment, *Phys. Rev. E* **102**, 012109 (2020).
- [35] T. O. E. Skinner, S. K. Schnyder, D. G. A. L. Aarts, J. Horbach, and R. P. A. Dullens, Localization dynamics of fluids in random confinement, *Phys. Rev. Lett.* **111**, 128301 (2013).
- [36] D. Wang, H. Wu, L. Liu, J. Chen, and D. K. Schwartz, Diffusive escape of a nanoparticle from a porous cavity, *Phys. Rev. Lett.* **123**, 118002 (2019).
- [37] J. Ślęzak and S. Burov, From diffusion in compartmentalized media to non-Gaussian random walks, *Sci. Rep.* **11**, 1 (2021).
- [38] J. M. Miotto, S. Pigolotti, A. V. Chechkin, and S. Roldán-Vargas, Length scales in Brownian yet non-Gaussian dynamics, *Phys. Rev. X* **11**, 031002 (2021).
- [39] E. M. Peterson, M. W. Manhart, and J. M. Harris, Single-molecule fluorescence imaging of interfacial DNA hybridization kinetics at selective capture surfaces, *Anal. Chem.* **88**, 1345 (2016).
- [40] T. Scholz and E. Mandelkow, Transport and diffusion of Tau protein in neurons, *Cell. Mol. Life Sci.* **71**, 3139 (2014).
- [41] M. Mercken, I. Fischer, K. S. Kosik, and R. A. Nixon, Three distinct axonal transport rates for tau, tubulin, and other microtubule-associated proteins: evidence for dynamic interactions of tau with microtubules in vivo, *J. Neurosci.* **15**, 8259 (1995).
- [42] T. E. Kreis and W. Birchmeier, Microinjection of Fluorescently Labeled Proteins into Living Cells with Emphasis on Cytoskeletal Proteins, *Int. Rev. Cytol.* **75**, 209 (1982).
- [43] S. K. Ghosh, A. G. Cherstvy, and R. Metzler, Non-universal tracer diffusion in crowded media of non-inert obstacles, *Phys. Chem. Chem. Phys.* **17**, 1857 (2015).

- [44] M. Javanainen, H. Hammaren, L. Monticelli, J.-H. Jeon, M. S. Miettinen, H. Martinez-Seara, R. Metzler, and I. Vattulainen, Anomalous and normal diffusion of proteins and lipids in crowded lipid membranes, *Faraday Discuss.* **161**, 397 (2013).